

VIBRATIONAL LEVEL POPULATION OF H<sub>2</sub> AND H<sub>2</sub><sup>+</sup> IN THE EARLY UNIVERSECARLA M. COPPOLA<sup>1,2</sup>, SAVINO LONGO<sup>1,3</sup>, MARIO CAPITELLI<sup>1,3</sup>, FRANCESCO PALLA<sup>4</sup>, DANIELE GALLI<sup>4</sup>*published on The Astrophysical Journal Supplement Series, 193:7 (11pp), 2011 March*

## ABSTRACT

We formulate a vibrationally resolved kinetics for molecular hydrogen and its cation in the primordial Universe chemistry. Formation, destruction and relaxation processes for each vibrational level are studied and included as chemical pathways of the present model. The fractional abundance of each vibrational level as a function of the redshift is given: a strong deviation from the Boltzmann distribution is found at low  $z$ . A discussion of the results is provided, also evaluating the effects of relaxation processes on the level populations. Analytical fits for some LTE rate coefficients are given in the Appendix.

*Subject headings:* cosmology: early Universe — methods: numerical — physical data and processes

## 1. INTRODUCTION

The primordial gas after recombination was composed of neutral hydrogen and helium atoms with traces of electrons, deuterium and lithium, exposed to the radiation field of the cosmic background radiation (hereafter CBR), and in adiabatic expansion. In these conditions, only a limited number of gas-phase reactions was possible. The first molecules started to form only ten thousand years after the Big Bang, at a redshift  $z \approx 2000$ , reaching a freeze-out abundance at  $z \approx 100$ : about  $10^{-6}$  for H<sub>2</sub>, followed by HD, H<sub>2</sub><sup>+</sup>, HeH<sup>+</sup> and several less abundant species (see Lepp et al. 2002 for a review).

Despite the simple chemical composition, the kinetics of elementary processes in the early Universe is very complex, due to the presence of a large number of quantum states for atoms and molecules involved in the network processes, including the interaction with the CBR. Detailed calculations of molecule formation in the early Universe have been recently performed by Hirata & Padmanabhan (2006, hereafter HP06), Puy & Signore (2007), Glover & Jappsen (2007), Schleicher et al. (2008, hereafter S08), and Vonlanthen et al. (2009, hereafter V09). In addition to these studies, comprehensive collections of analytic fits of chemical reaction rates were also given by Anninos & Norman (1996), Stancil et al. (1998), Galli & Palla (1998, hereafter GP98) and, more recently, by Glover & Abel (2008).

In studies of primordial chemistry, the rovibrational levels manifold of the molecules has been usually ignored, mainly because of the lack of state-to-state resolved cross sections (or, equivalently, reaction rates) of the relevant chemical processes. Early estimates of the vibrational distribution function of H<sub>2</sub> attempted by means of physical order-of-magnitude arguments (Khersonskii 1982) led to the conclusion that the vibrationally excited states of H<sub>2</sub> are rapidly deactivated through radiative decay. This is because the H-H<sub>2</sub> collision time is much longer than

the radiative lifetime of vibrational levels, so that the population of the vibrational levels is essentially determined by the Einstein coefficients and the probability of formation of vibrationally excited H<sub>2</sub> molecules. HP06 were the first to compute in detail the vibrational level populations of H<sub>2</sub><sup>+</sup>. However, they did not consider collisional processes inducing vibrational relaxation.

Because of these simplifications, chemical reaction rates are usually evaluated under the hypothesis of local thermal equilibrium (hereafter LTE). However, non-equilibrium distribution function can significantly affect the results of such calculations, as shown explicitly by Capitelli et al. (2007) for the dissociative attachment process of H<sub>2</sub>. This evidence suggests that the evaluation of the exact vibrational distribution function is necessary to model the plasma kinetics, as pointed out by Lepp et al. (2002). The relatively simple internal structure of atomic and molecular hydrogen, and its molecular cation H<sub>2</sub><sup>+</sup>, makes possible such a *state-to-state* approach at least for these species.

In the present work, we follow for the first time the chemical composition of the primordial gas, determining the population of vibrational levels of H<sub>2</sub> and H<sub>2</sub><sup>+</sup>, adopting a detailed network of formation and destruction channels and relaxation processes, such as radiative and atom/ion-molecule collisions. We ignore any contribution due to subsequent astrophysical processes that affect the chemical composition of the gas such as primordial massive supernovae, which, besides providing heavy elements, may also contribute to the formation of H<sub>2</sub> in the early Universe (Cherchneff & Lilly 2008).

The paper is organized as follows: in Section 2 we discuss the relevant vibrationally resolved reactions and we compute state-to-state reaction rate coefficients; in Section 3 we describe our chemical network; in Section 4 we present our results for the evolution of the vibrational level populations of H<sub>2</sub> and H<sub>2</sub><sup>+</sup>; finally, in Section 5 we summarize our conclusions. In the Appendix, we give a list of fitting formulae for specific rate coefficients under LTE conditions.

2. VIBRATIONALLY RESOLVED REACTION RATES FOR H<sub>2</sub> AND H<sub>2</sub><sup>+</sup>

In a hydrogen plasma, H<sub>2</sub> and H<sub>2</sub><sup>+</sup> form by various collision processes, generally in vibrationally excited states.

<sup>1</sup> Università degli Studi di Bari, Dipartimento di Chimica, Via Orabona 4, I-70126 Bari, Italy

<sup>2</sup> Department of Physics and Astronomy, University College London, Gower Street, London WC1E 6BT

<sup>3</sup> IMP-CNR, Section of Bari, via Amendola 122/D, I-70126 Bari, Italy

<sup>4</sup> INAF-Osservatorio Astrofisico di Arcetri, Largo E. Fermi 5, I-50125 Firenze, Italy

TABLE 1  
VIBRATIONALLY RESOLVED REACTIONS INCLUDED IN THIS WORK

Chemical process	Reference
1] $\text{H} + \text{H}_2(v) \rightarrow \text{H} + \text{H}_2(v')$	(1)
2] $\text{H} + \text{H}_2(v) \rightarrow \text{H} + \text{H} + \text{H}$	(1)
3] $\text{H} + \text{H}^- \rightarrow \text{H}_2(v) + e^-$	(2)
4] $\text{H} + \text{H}^+ \rightarrow \text{H}_2^+(v) + h\nu$	detailed balance from (6)
5] $\text{H}_2^+(v) + \text{H} \rightarrow \text{H}_2(v') + \text{H}^+$	(3)
6] $\text{H}_2(v) + \text{H}^+ \rightarrow \text{H}_2^+(v') + \text{H}$	(3)
7] $\text{H}_2^+(v) + \text{H} \rightarrow \text{H}_2^+(v') + \text{H}$	(3)
8] $\text{H}_2(v) + \text{H}^+ \rightarrow \text{H}_2(v') + \text{H}^+$	(3)
9] $\text{H}_2^+(v) + \text{H} \rightarrow \text{H}^+ + \text{H} + \text{H}$	(4)
10] $\text{H}_2(v) + \text{H}^+ \rightarrow \text{H} + \text{H} + \text{H}^+$	(4)
11] $\text{H}_2(v) + h\nu \rightarrow \text{H}_2^+(v') + e^-$	(5)
12] $\text{H}_2^+(v) + h\nu \rightarrow \text{H} + \text{H}^+$	(6)
13] $\text{H}_2(v) + h\nu \rightarrow \text{H} + \text{H}$	direct + indirect (7)
14] $\text{H}_2^+(v) + e^- \rightarrow \text{H} + \text{H}$	(8)
15] $\text{H}_2(v) + e^- \rightarrow \text{H}^- + \text{H}$	(9)
16] $\text{H}_2(v) + e^- \rightarrow \text{H}_2(v') + e^- + h\nu$	(9)
17] $\text{H}_2(v) \rightarrow \text{H}_2(v') + h\nu$	(10)
18] $\text{H}_2^+(v) \rightarrow \text{H}_2^+(v') + h\nu$	(11)
19] $\text{HeH}^+ + \text{H} \rightarrow \text{H}_2^+(v) + \text{He}$	(12)

References: (1) Esposito et al. (1999, 2001); (2) Čížek et al. (1998); (3) Krstić et al. (1999, 2002), Krstić (2002); (4) Krstić (2003); (5) Flannery et al. (1977); (6) Dunn (1968); (7) Allison & Dalgarno (1969, 1970), Dalgarno & Stephens (1970); (8) Takagi (2002); (9) Celiberto et al. (2001); (10) Wolniewicz et al. (1998); (11) Posen et al. (1983); (12) Linder et al. (1995) (see S08).

For example, in the case of  $\text{H}_2^+(v)$ , the electron impact ionization process produces a known population of vibrational states given by the corresponding Franck-Condon factors for the transitions. For other formation processes,  $\text{H}_2^+(v)$  is created with different populations of vibrational levels. Additionally, inelastic collisions with other plasma constituents strongly affect the evolution and thermalization of vibrational levels of  $\text{H}_2$  and  $\text{H}_2^+$ . This fact underlines the importance of such a vibrationally resolved kinetics, since a priori assumptions and approximations could fail in evaluating the vibrational level distribution.

Typically, collisional processes in a low-temperature plasma involve all molecular degrees of freedom (electronic, vibrational and rotational); however, in order to model the kinetics of vibrational levels of  $\text{H}_2$  and  $\text{H}_2^+$ , rotational equilibrium has been assumed.

For processes not involving  $\text{H}_2$  and  $\text{H}_2^+$ , we have adopted the chemical network recently developed by S08, updating the value of the rate coefficient for the  $\text{H}^-$  photodetachment to include the contribution of non-thermal photons due to cosmological H and He recombination (see HP06). The corresponding rate coefficient for this process is given in Table 3. For  $\text{H}_2$  and  $\text{H}_2^+$ , we computed state-to-state rate coefficients from available cross sections, including all vibrational levels of their fundamental electronic states (15 and 19 states, respectively).

A list of the chemical processes included in our calculation is shown in Table 1. Each process will be described separately in the following subsections.

### 2.1. Associative detachment

The importance of the reaction of associative detachment for  $\text{H}^-$ ,

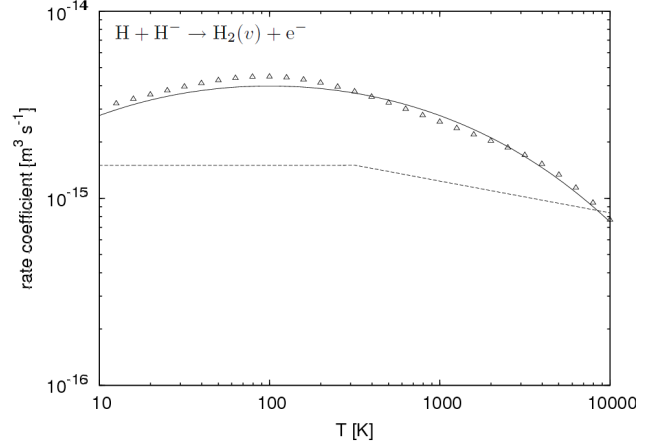
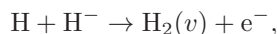


FIG. 1.—  $\text{H}-\text{H}^-$  associative detachment rate coefficient. *Triangles*, total rate coefficient obtained from the cross sections of Čížek et al. (1998), according to Eq. (1); *dashed curve*, fit by GP98 of the total rate coefficient from Launay et al. (1991); *solid curve*, fit reported in Table 3.

was first pointed out by Dalgarno (quoted by Pagel 1959). Various studies have been published on the vibrationally resolved cross sections and/or rate coefficients for this process (Bieniek & Dalgarno 1979, Launay et al. 1991), underlying the importance of this channel of  $\text{H}_2$  formation (e.g. Dalgarno 2005; Flower 2000).

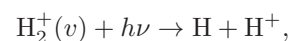
Our calculations are based on the detailed data by Čížek et al. (1998). These authors developed an improved nonlocal resonance model for the description of the nuclear dynamics of the  $\text{H}_2^-$  collision complex, and calculated both associative detachment and dissociative attachment cross sections. They provide data for different values of the angular momentum  $J$  of the  $\text{H}^- + \text{H}$  collision<sup>5</sup>. For each initial angular momentum, the  $\text{H}_2$  molecule can be produced in states with the rotational quantum number equal to  $J+1$  or  $J-1$  due to selection rules; states with the same  $J$  are not allowed by symmetry conditions on the total wavefunction and higher changes in  $J$  are neglected in their model. The total rate coefficient, obtained as a sum of the vibrationally resolved rate coefficients,

$$k_{\text{tot}}(T_{\text{gas}}) = \sum_v k_v(T_{\text{gas}}), \quad (1)$$

is shown in Fig. 1, compared with the rate coefficient computed by Launay et al. (1991), as fitted by GP98. The new fit is given in Table 3. Using this rate coefficient in a non-vibrationally resolved chemical network of the primordial Universe has a negligible impact on the  $\text{H}_2$  abundance. Indeed, this reaction is also one of the most important  $\text{H}^-$  loss channel. Therefore increasing the associative detachment rate coefficient cannot lead to a production rate of  $\text{H}_2$  faster than the  $\text{H}^-$  production rate. For the same reasons,  $\text{H}^-$  fraction is reduced accordingly, by a factor of 4.

### 2.2. Photodissociation of $\text{H}_2^+(v)$

The photodissociation of  $\text{H}_2^+(v)$ ,



<sup>5</sup> Data in electronic format are available at [http://utf.mff.cuni.cz/~cizek/AD\\_H2/](http://utf.mff.cuni.cz/~cizek/AD_H2/).

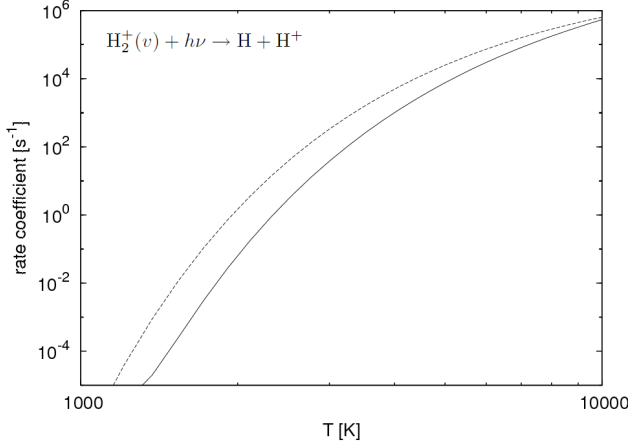
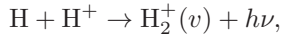


FIG. 2.— H<sub>2</sub><sup>+</sup> photodissociation rate coefficient. *Solid curve*, total rate in LTE, summed over all possible initial, from the cross sections by Dunn 1968; *dashed curve*, fit by GP98 based on data by Argyros (1974) and Stancil (1994).

is a typical example of direct process of photodestruction. Lebedev et al. (2000, 2003) provided a significant analysis of bound-free (including also photodissociation) and free-free transitions for H<sub>2</sub><sup>+</sup>(*v*), limited however to sums on the rotational and vibrational quantum numbers. In this work, we have adopted the vibrationally resolved cross sections calculated by Dunn (1968), evaluated fixing the rotational quantum number  $J = 1$ . The comparison between the LTE rate coefficient obtained using the vibrationally resolved data by Dunn and the fit by GP98 of data by Argyros (1974) for  $2500 \text{ K} < T_{\text{rad}} < 26000 \text{ K}$  and by Stancil (1994) for  $3150 \text{ K} < T_{\text{rad}} < 25200 \text{ K}$  is shown in Fig. 2.

### 2.3. Radiative association of H and H<sup>+</sup>

The reaction of radiative association of H and H<sup>+</sup>,



has been the subject of several studies (e.g., Ramaker & Peek 1976, Shapiro & Kang 1987, Stancil et al. 1993). However, no vibrationally resolved data are available in literature. For this reason, we have applied the principle of detailed balance to the inverse H<sub>2</sub><sup>+</sup>(*v*) photodissociation reaction,

$$k_v^{\text{rad.ass.}} = \frac{Z_{\text{H}_2^+(v)}}{Z_{\text{H}}Z_{\text{H}^+}} e^{h\nu_v/kT_{\text{rad}}} k_v^{\text{ph.}} \quad (2)$$

where  $T_{\text{rad}}$  is the temperature of the CBR,  $h\nu_v$  is the thermal threshold for the *v*-th level. The partition functions  $Z$  of reagents and product are

$$Z = \frac{(2\pi kT_{\text{gas}})^{3/2}}{h^3} \begin{cases} m_{\text{H}}^{3/2} g_{\text{H}} Q_{\text{H}} & \text{for H,} \\ m_{\text{H}^+}^{3/2} g_{\text{H}^+} & \text{for H}^+, \\ m_{\text{H}_2^+}^{3/2} g_{\text{H}_2^+} Q_{\text{H}_2^+} Z_{\text{rot}}(v, T_{\text{gas}}) & \text{for H}_2^+(v), \end{cases}$$

where  $g_{\text{H}}$ ,  $g_{\text{H}^+}$  and  $g_{\text{H}_2^+}$  are the multiplicities of the nuclear spin contributions for H, H<sup>+</sup> and H<sub>2</sub><sup>+</sup>, equal to  $g_{\text{H}} = g_{\text{H}^+} = 2 \times (1/2) + 1 = 2$  and  $g_{\text{H}_2^+} = 4$ ;  $Q_{\text{H}}$  and  $Q_{\text{H}_2^+}$  are the electron spin degeneracies, equal to 2 both for H and H<sub>2</sub><sup>+</sup> under the hypothesis that only their ground electronic states contribute to the partition function and  $Z_{\text{rot}}(v, T_{\text{gas}})$  is the rotational partition function,

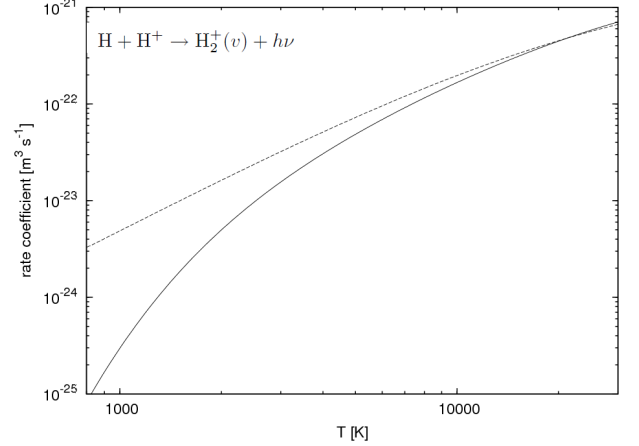


FIG. 3.— H-H<sup>+</sup> radiative association rate coefficient. *Solid curve*, total rate coefficient obtained using the detailed balance principle from the photodissociation data by Dunn (1968), according to Eq. (2); *dashed curve*, fit by GP98 of the total rate coefficient from Ramaker & Peek (1976), that takes into account the rotational structure of each vibrational level of the cation hydrogen molecule, given by

$$Z_{\text{rot}}(v, T_{\text{gas}}) = \sum_J g_J e^{-(E_0 - E_{vJ})/kT_{\text{gas}}},$$

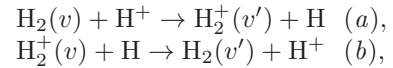
where  $E_{vJ}$  is the binding energy of the (*v*, *J*)-th level and  $E_0$  the binding energy of the lowest rovibrational level. The symbol  $g_J$  represents the multiplicity of each electronic-rotational level,

$$g_J = \begin{cases} \frac{1}{4}(2J+1) & \text{for } J \text{ even,} \\ \frac{3}{4}(2J+1) & \text{for } J \text{ odd.} \end{cases}$$

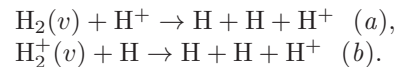
A comparison between the present LTE calculation and the fit by GP98 of data by Ramaker & Peek (1976) is shown in Fig. 3.

### 2.4. Charge transfer, collisional excitation, and dissociation

The H<sup>+</sup>-H<sub>2</sub> and the H-H<sub>2</sub><sup>+</sup> systems represent one of the most important collision complexes in the hydrogen plasma, called in short the H<sub>3</sub><sup>+</sup> collision system. In addition to elastic collisions H<sub>2</sub>-H<sup>+</sup> and H<sub>2</sub><sup>+</sup>-H, the relevant reactions are: (i) charge transfer,



and (ii) collisional dissociation,



The most complete theoretical work describing these chemical reaction pathways has been recently developed by Krstić and collaborators (Krstić 2002, 2003, 2005; Krstić et al. 1999, 2002) within the *infinite order sudden approximation* method (IOSA)<sup>6</sup>. As described by Krstić et al. (2002), charge transfer (a) is endoergic for  $v \leq 3$ , although with low threshold energies, and is strictly competitive with the vibrational excitation channel, especially for those states than can overcome the kinetic barrier ( $v \geq 4$ ). For higher vibrational levels, the process

<sup>6</sup> Data in electronic form are available at <http://www-cfadc.phy.ornl.gov/astro/ps/data/home.html>.

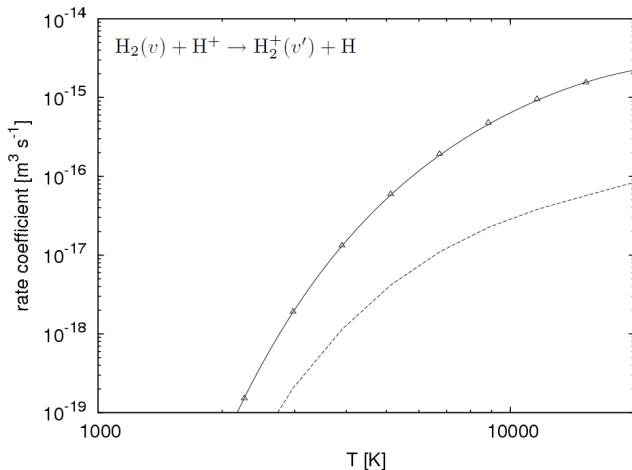


FIG. 4.—  $\text{H}_2\text{-H}^+$  charge transfer rate coefficient. *Triangles*, total rate in LTE, summed over all possible initial and final states, from the cross sections of Krstić (2002) and Krstić et al. (2002, 2003); *dashed curve*, fit by Savin et al. (2004) for  $\text{H}_2(v=0)$ ; *solid curve*, fit listed in Table 3.

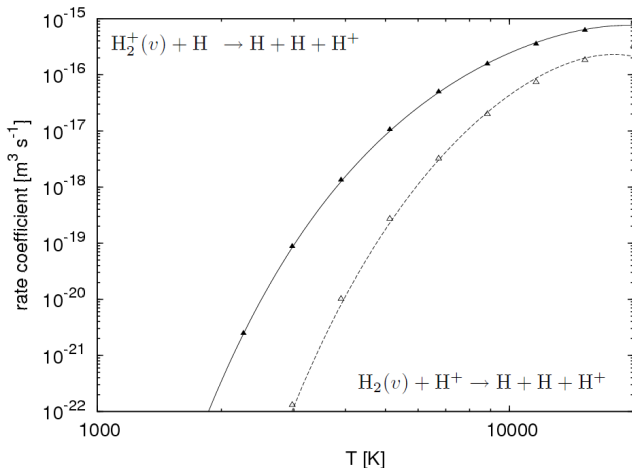


FIG. 5.—  $\text{H}_2^+\text{-H}$  (filled triangles) and  $\text{H}_2\text{-H}^+$  (open triangles) total dissociation rate coefficients in LTE, summed over all possible initial and final states, from the cross sections of Krstić (2002) and Krstić et al. (2002, 2003). The fits listed in Table 3 are also shown as solid and dashed lines, respectively.

is exoergic, as the process of charge transfer (b), for all  $v$ . The LTE rate coefficient for the charge exchange reaction (a) is shown in Fig. 4, and compared with the fit by Savin et al. (2004) for  $\text{H}_2(v=0)$ . For the reaction (b), cross-sections have been extrapolated at low energies using a Langevin-type power law; the resulting rate coefficients have been scaled in order to obtain an LTE value corresponding to the experimental measurement by Karpas et al. 1979 at  $T_{\text{gas}} = 300$  K. The rate coefficients for the collisional dissociation reactions (a) and (b) are shown in Fig. 5. The fits are given in Table 3.

### 2.5. $\text{H}_2/\text{H}$ vibrational-translational transfer

Elastic collisions among hydrogen atoms and molecules deeply modify the initial vibrational distribution function of molecular components in a hydrogen plasma. They are generally classified as V-T (vibrational-translational) and V-V (vibrational-vibrational) processes. In the former case, energy transfer between the translational degree of freedom of the colliding atom and

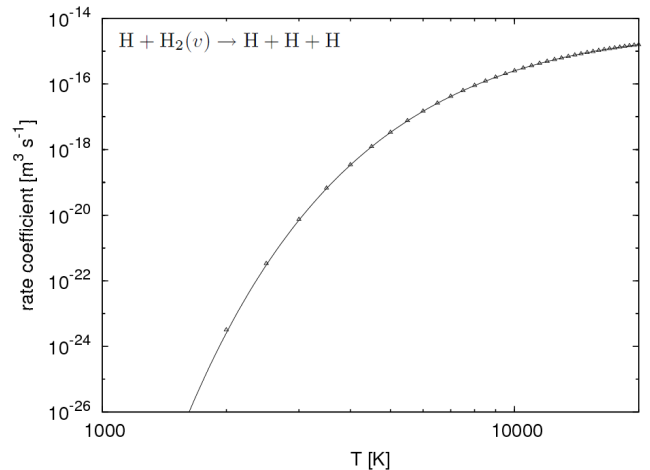
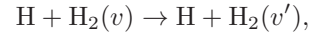


FIG. 6.—  $\text{H}_2$  dissociation by H impact: *Triangles*: rate coefficient computed from the cross sections of Esposito et al. (1999); *solid line*: fit reported in Table 3.

the vibrational state of the target molecule occurs; the latter represents the energy exchange between the vibrational manifolds of the colliding molecules. In both cases, multi-quantum transitions can occur, coupling the entire set of vibrational levels. Recently, Krstić et al. (2002) have calculated V-T cross sections for collisions between H and  $\text{H}_2$ ,

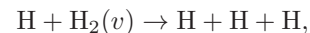


using the quantum mechanical IOSA method. However, while data are available for the collision system  $\text{H}^+ - \text{H}_2(v)$ , no state-to-state information on collisions among hydrogen atoms and molecules is available for all  $(v, v')$  pairs. The V-T rate coefficients used in the present work have been obtained from cross sections computed by Esposito et al. (1999, 2001) using the *quasiclassical trajectory* (QCT) method.

Collisions of  $\text{H}_2$  with He atoms have been studied by e.g. Clark (1997), Flower et al. (1998), Balkrishnan et al. (1999), Lee et al. (2005), but no data for each  $(v, v')$  pair are available. In this work we have neglected V-T processes with He. This assumption is based on the observation that vibrating nuclei in  $\text{H}_2$  are lighter than the colliding He atom; moreover, the relative abundance of He is small: for these reasons, the V-T transfer with He can be considered less efficient than V-T transfer with H. Also molecule-molecule collisions have been neglected, owing to the small fractional abundance of  $\text{H}_2$  with respect to H.

### 2.6. Collisional dissociation of $\text{H}_2$

The cross sections for the dissociation of  $\text{H}_2$  induced by collisions with H,



have been computed by Esposito et al. (1999, 2001) with the QCT method. The whole vibrational manifold of  $\text{H}_2$  has been explored. The total LTE rate coefficient is shown in Fig. 6, and the fit is given in Table 3.

### 2.7. Photoionization of $\text{H}_2$

Ionization of  $\text{H}_2$  can proceed through collisions with particles and photons. Data on ionization caused by electron impact are described by Liu & Shemansky (2004), and compared with photoionization data.



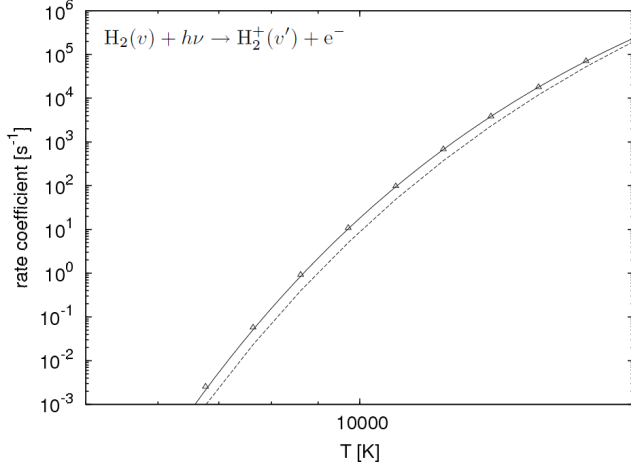
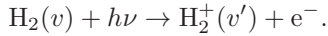


FIG. 7.— H<sub>2</sub> photoionization rate coefficient. *Triangles*, total rate in LTE, summed over all possible initial and final states, from the cross sections by Flannery et al. (1977); *dashed curve*, fit by GP98 based on data by O'Neil & Reinhardt (1978); *solid curve*, fit given in Table 3.

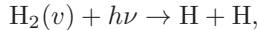
Because threshold energies for the electron-impact ionization cross sections are much higher than thermal energies available at the redshift range considered in the present work ( $E > 16$  eV vs.  $E < 2$  eV), we have considered only photoionization of H<sub>2</sub>,



Several theoretical calculations of H<sub>2</sub> photoionization have been proposed during the years (Lewis Ford et al. 1975, O'Neil & Reinhardt 1978). This chemical reaction couples each vibrational level of H<sub>2</sub> with each vibrational level of H<sub>2</sub><sup>+</sup>. Available data on vibrationally resolved ( $v, v'$ ) cross sections have been published by Flannery et al. (1977), following the theoretical and computational procedures described by Tai & Flannery (1977). Fig. 7 shows the comparison between the total photoionization rate coefficient calculated in the hypothesis of LTE using the cross sections by Flannery et al. (1977), whose fit is given in Table 3, and the fit by GP98 based on data by O'Neil & Reinhardt (1978).

### 2.8. Photodissociation of H<sub>2</sub>

Photodissociation of H<sub>2</sub>,



can occur both directly (absorption from a lower level into the continuum) or indirectly (the so-called “Solomon process”), a process consisting in the absorption into an individual level of a bound upper state, followed by dissociation. In the present work, we considered both destruction pathways. For the direct process, vibrationally resolved rate coefficients are given by

$$k_v^{\text{ph.}}(T_{\text{rad}}) = 4\pi \int_0^\infty \frac{\sigma_v^{\text{ph.}}(\nu)}{h\nu} J_\nu(T_{\text{rad}}) d\nu, \quad (3)$$

where the cross sections  $\sigma_v^{\text{ph.}}$  are taken from the work by Allison & Dalgarno (1969). More recently, new calculations of photodissociation cross sections have been published by Glass-Maujean (1986) and Zucker & Eyler (1986), including excited electronic states; however, no significant changes have been introduced for the Lyman and Werner systems. A thorough analysis

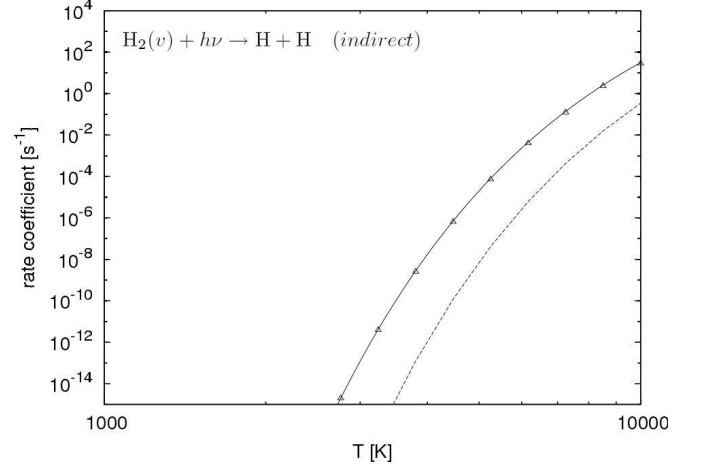


FIG. 8.— H<sub>2</sub> indirect photodissociation rate coefficient. *Triangles*, total rate in LTE, both considering the Lyman and the Werner system, obtained using Eq. (4) and data by Dalgarno & Stephens (1970) and Allison & Dalgarno (1970); *dashed curve*, fit by S08 on Glover & Jappsen (2007) data; *solid curve*, fit given in Table 3.

of the direct process with related fits and reaction rates for the kinetics of the early Universe is given in Coppola et al. (2011).

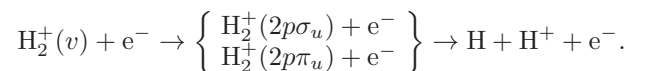
For the calculation of the rate coefficient of the indirect process, we have used the discrete version of Eq. (3)

$$k_v^{\text{ph.}}(T_{\text{rad}}) = \frac{\pi e^2}{m_e c^2} \lambda_{uv}^2 f_{uv} \epsilon_u J_{\lambda_{uv}}(T_{\text{rad}}), \quad (4)$$

where  $u$  is the vibrational level of both Lyman and Werner electronically excited intermediate systems, whose dissociation efficiencies  $\epsilon_u$  have been taken from Dalgarno & Stephens (1970). The oscillator strengths  $f_{uv}$  for the same molecular states have been calculated by Allison & Dalgarno (1970), and the vibrational energies of both Lyman and Werner states by Fantz & Wunderlich (2006). In Fig. 8 we show the comparison between the fit of the rate coefficient by S08 of the data by Glover & Jappsen (2007) and the total LTE rate coefficient obtained using Eq. (4). The present calculation includes both Lyman and Werner systems, and the contribution of the total vibrational manifold has been considered.

### 2.9. Dissociative excitation and dissociative recombination of H<sub>2</sub><sup>+</sup>

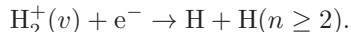
The fate of the dissociative scattering processes between electrons and H<sub>2</sub><sup>+</sup> strictly depends on the energy of the collision. The effectiveness of these chemical reactions is connected to the energy thresholds of the vibrational states of the intermediate excited states: at high collision energies, the favored dissociative channel is dissociative excitation (DE):



However, experimental evidence (Yousif & Mitchell 1995) has shown that large DE cross sections are operative at energies  $\sim 0.01$  eV. For this reason, other reaction pathways become important at these energies, involving electron capture into excited electronic states of H<sub>2</sub>. In particular, H<sub>2</sub>(<sup>1</sup>Σ<sub>g</sub><sup>+</sup>) or auto-ionizing dissociative Rydberg

states lying below the  $H_2^+(2p\sigma_u)$ , both auto-ionizing in the continuum of  $H_2^+$ , have been considered in the dynamical mechanisms of dissociative excitation.

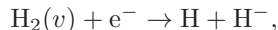
At low energies, DE processes are competitive with dissociative recombination (DR), in which the incident electron is temporally captured into the Rydberg state by transferring its kinetic energy to vibrational motion. The unstable molecule can dissociate or go back to the ionizing state by an elastic or vibrational transition. This mechanism is sometimes called “indirect process” of DR. In the direct process, excited hydrogen molecules dissociate in the vibrational continuum of  $H_2$ . In this case, two H atoms are produced, one in the ground electronic state, the other in states with principal quantum number  $n \geq 2$ :



Different studies have focused on DE and/or DR of  $H_2^+$  (e.g., Takagi 2002; Stroe & Fofirig 2009; Fofirig & Stroe 2008; Motapon et al. 2008; Takagi et al. 2009). We have used data from the work by Takagi (2002), where DR and DE cross sections have been calculated using the *multi-quantum defect theory* (MQDT). For each vibrational level, Takagi (2002) provided both DR and DE cross sections. All excited dissociative states are included (all Rydberg states of 5 different symmetries) and for the lowest dissociative state, the electronic interaction is fully taken into account. Fig. 9 shows the comparison between the total dissociative recombination rate coefficient calculated in the hypothesis of LTE using the cross sections by Takagi (2002), and the fit by GP98 based on data by Schneider et al. (1994). Our fit is given in Table 3. Although the cross sections of this process have a threshold component which corresponds to a repulsive channel, the threshold feature is located at too high energy to affect results in the present application. The main features relevant here are instead the presence of many resonances at low energy which convolute into a strongly decreasing trend for energies below a few eV, and a global increase of this low energy portion of the cross sections with  $v$ . As a result, the LTE rate coefficient decreases with  $T_{\text{gas}}$  until a few thousand K, where the raising population of vibrational levels reverses this trend. The fit by GP98, reported in Fig. 9 for reference, was based on data by Schneider et al. (1994), given up to  $T_{\text{gas}} = 4000$  K and therefore showed a monotonic trend.

#### 2.10. Dissociative attachment

Electron-impact inelastic processes of vibrationally excited  $H_2$  molecules,



play an important role in the kinetics of a low-temperature hydrogen plasma. Especially for inelastic collisions involving an electronic transition, two important features can be noted: if a vibrationally excited molecule is involved, the threshold decreases and the cross section of the process increases (for some processes dramatically) with increasing vibrational excitation of the molecule. In this work we have used data calculated by Celiberto et al. (2001), based on an improved version of the resonant scattering model originally developed by Fano (1961). The dynamics of this route provides for the formation of a temporary negative molecular ion,

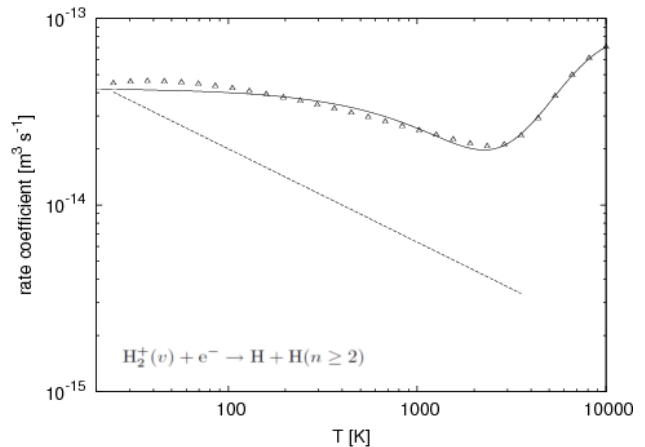
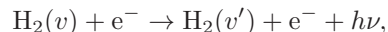


FIG. 9.—  $H_2^+$  dissociative recombination rate coefficient. *Triangles*, total rate in LTE, summed over all initial states, from the cross sections by Takagi (2002); *dashed curve*, fit by GP98 based on data by Schneider et al. (1994), given in the temperature range  $20 \text{ K} < T_{\text{gas}} < 4000 \text{ K}$ ; *solid curve*, fit reported in Table 3.

whose fate is either ionization or dissociation. The fit of the LTE rate coefficient can be found in Capitelli et al. (2007).

#### 2.11. Electron collisional excitation of $H_2$

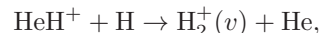
The process of vibrational excitation of molecules by electron collisions,



also known as the E-V process, selectively populates high vibrational levels and represents one of the main non-equilibrium pathways in the vibrational kinetics of hydrogen plasma. It is a two-step process that links a vibrational state of the electronic ground state to another vibrational state of the same manifold, via an intermediate singlet state that can radiatively decay. As in the case of dissociative attachment, we have used data from Celiberto et al. (2001).

#### 2.12. Formation of $H_2^+$ via $HeH^+$

The  $HeH^+$  channel for the formation of  $H_2^+(v)$ ,



has been considered in several studies (e.g. Dalgarno 2005, HP06, S08). The rate coefficient usually adopted in these kinetics models is estimated from the experimental work by Karpas et al. (1979) or data by Linder et al. (1995). However, no vibrationally resolved information is available. In order to overcome this limitation, we follow here an approach similar to that of Hirata & Padmanabhan (2006), where this reaction is assumed to equally populate all levels compatible with energy balance, i.e. all levels with energy  $E < -1.844 \text{ eV}$  with respect to the  $H_2^+$  dissociation limits. Since in the present work individual rovibrational levels are not considered, we follow a simplified approach by assuming that this reaction channel produces  $H_2^+$  molecules in the first three vibrational levels with equal rates.

#### 2.13. Radiative transitions of $H_2$

Quadrupolar transition probabilities for H<sub>2</sub>(*v*) have been calculated by Wolniewicz et al. (1998)<sup>7</sup>. The authors improved earlier calculations by Turner et al. (1977) by adopting a more accurate potential energy curve, providing tables for the spontaneous decay from an initial to a final vibrational level for  $\Delta J = 0, \pm 2$ . The rovibrational energy levels used to perform the sum of available transition rates have been calculated using the WKB method (Esposito 2010, priv. comm.). They are in very good agreement with classical calculations by Kolos & Wolniewicz (1964).

### 2.14. Radiative transitions of H<sub>2</sub><sup>+</sup>

Calculations of quadrupole transition probabilities for H<sub>2</sub><sup>+</sup>(*v*) follow the method used by Wolniewicz et al. (1998) for H<sub>2</sub>. Radiative transitions for H<sub>2</sub><sup>+</sup> have been calculated by Posen et al. (1983) for vibrational-vibrational transitions at given *J* and  $\Delta J$ . The energies of the rovibrational levels used to perform the sum have been calculated by Hunter et al. (1974).

## 3. CHEMICAL NETWORK

To describe the time evolution of the chemical species during the expansion of the Universe, we solve numerically the system of ODEs

$$\begin{aligned} \frac{dn_v}{dt} = & -n_v \sum_{v'} (R_{vv'} + P_{vv'} + C_{vv'} n_{v'}) + \\ & + \sum_{v'} R_{vv'} n_{v'} + \sum_{v'} \sum_{v''} C_v^{v'v''} n_{v'} n_{v''}. \end{aligned} \quad (5)$$

where  $R_{vv'}$  are the spontaneous and stimulated radiative rate coefficients;  $P_{vv'}$  are the destruction rate coefficients of the *v*-th species by photons;  $C_{vv'}$  are the destruction rate coefficients for the *v*-th species for collisions with the *v'*-th chemical partner; and  $C_v^{v'v''}$  are the formation rate coefficients of the *v*-th species due to collisions between the *v'*-th and *v''*-th species, photons included.

The radiative rate coefficients are related to the Einstein coefficients by

$$\begin{aligned} R_{vv'} &= \begin{cases} A_{vv'} B_{vv'} u(\nu_{vv'}, T_{\text{rad}}) & \text{if } v' < v \\ B_{vv'} u(\nu_{vv'}, T_{\text{rad}}) & \text{if } v' > v, \end{cases} \\ &= \begin{cases} A_{vv'} [1 + \eta(\nu_{vv'}, T_{\text{rad}})] & \text{if } v' < v \\ g_{v'} A_{v'v} \eta(\nu_{vv'}, T_{\text{rad}}) / g_v & \text{if } v' > v \end{cases} \end{aligned}$$

where  $\nu_{vv'}$  is the frequency of the transition  $v \rightarrow v'$ ,  $g_v = 1$  is statistical weight of the *v*-th level,  $u(\nu_{vv'}, T_{\text{rad}})$  is the Planck photon distribution, and  $\eta(\nu_{vv'}, T_{\text{rad}}) = [\exp(h\nu_{vv'}/kT_{\text{rad}}) - 1]^{-1}$ .

The chemical network is completed by the equations for the gas and radiation temperature evolutions and the equation for the redshift,

$$\frac{dt}{dz} = -\frac{1}{(1+z)H(z)}, \quad (6)$$

where

$$H(z) = H_0 \sqrt{\Omega_r(1+z)^4 + \Omega_m(1+z)^3 + \Omega_K(1+z)^2 + \Omega_\Lambda}. \quad (7)$$

The number density of hydrogen atoms is

$$n_H = \Omega_b \frac{3H_0^2}{8\pi G m_H} (1 - Y_p)(1+z)^3, \quad (8)$$

where  $\Omega_b$  is the baryon fraction,  $Y_p$  is the helium mass fraction,  $G$  is the constant of gravitation and  $m_H$  the atomic hydrogen mass.

Numerical values of the cosmological parameters  $H_0$ ,  $T_0$ ,  $\Omega_r$ ,  $\Omega_m$ ,  $\Omega_b$ ,  $\Omega_\Lambda$  and  $Y_p$  have been obtained from WMAP5 data (Komatsu et al. 2009, see Table 2). The initial fractional abundances for H, He and D are also listed in the same table. The hydrogen ionization fraction was computed using the routine RECFAST (Seager et al. 1999, Seager et al. 2000, Wong et al. 2008). Helium was assumed to be fully neutral in the redshift range of interest ( $z \leq 2000$ ). The electron density was determined by imposing the condition of charge neutrality. Atomic and molecular weights were taken from the NIST webpage<sup>8</sup>.

TABLE 2  
COSMOLOGICAL PARAMETERS

Cosmological parameter	Numerical value
$H_0$	100 h km s <sup>-1</sup> Mpc <sup>-1</sup>
$h$	0.705
$z_{\text{eq}}$	3141
$T_0$	2.725 K
$\Omega_{\text{dm}}$	0.228
$\Omega_b$	0.0456
$\Omega_m$	$\Omega_{\text{dm}} + \Omega_b$
$\Omega_r$	$\Omega_m / (1 + z_{\text{eq}})$
$\Omega_\Lambda$	0.726
$\Omega_K$	$1 - \Omega_r - \Omega_m - \Omega_\Lambda$
$Y_p$	0.24
$f_H$	0.924
$f_{\text{He}}$	0.076
$f_D$	$2.38 \times 10^{-5}$

Data tables of vibrationally resolved rate coefficients have been inserted as input of the routine LSODE<sup>9</sup> used to integrate the chemical system, which consists of 47 differential equations, one for each chemical species introduced in the model and one for the gas temperature. An implicit method has been used to perform the integration, being the kinetic problem stiff. Linear interpolation of the rate coefficients and of the ionization fraction is performed in logarithmic scale at each step of integration.

## 4. RESULTS AND DISCUSSION

The resulting fractional abundances of H<sub>2</sub> and H<sub>2</sub><sup>+</sup> for each vibrational level are shown as a function of redshift in Fig. 10. The total fractional abundance of H<sub>2</sub> shows a rapid increase at three epochs: at  $z \approx 1500$  by the charge transfer channel, dominant at high temperatures, at  $z \approx 300$  by H<sub>2</sub><sup>+</sup> radiative association formation, that modulates the charge transfer channel, and at  $z \approx 100$  by the associative detachment process. At  $z = 10$  the fractional abundances of H<sub>2</sub> and H<sub>2</sub><sup>+</sup> are  $5.76 \times 10^{-7}$  and  $6.56 \times 10^{-14}$ , respectively. Our value of the H<sub>2</sub> abundance is in good agreement with that obtained by HP06

<sup>7</sup> Data in electronic format are available at <http://cfa-www.harvard.edu/~simbotin/4pole.html>.

<sup>8</sup> <http://webbook.nist.gov/chemistry/name-ser.html>

<sup>9</sup> [https://computation.llnl.gov/casc/odepack/download/lode\\_agree.html](https://computation.llnl.gov/casc/odepack/download/lode_agree.html)

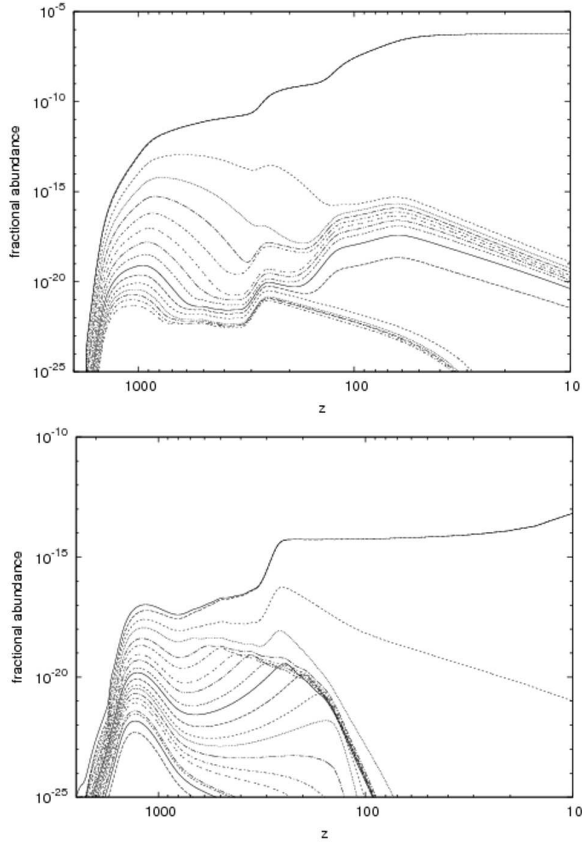


FIG. 10.— Vibrational level populations of  $\text{H}_2$  (top panel, from  $v = 0$  to  $v = 14$ ) and  $\text{H}_2^+$  (bottom panel, from  $v = 0$  to  $v = 18$ ) as function of redshift. In both cases, the solid curve shows the total fractional abundance.

( $f(\text{H}_2) = 6.0 \times 10^{-7}$  at  $z = 20$ ) but about twice the value of V09 ( $2.7 \times 10^{-7}$  at  $z = 10$ ). As for  $\text{H}_2^+$ , our abundance is in good agreement with the result of V09 ( $f(\text{H}_2^+) = 6.7 \times 10^{-14}$  at  $z = 10$ ), whereas HP06 obtain three different abundances depending on the value of the  $\text{H}_2^+ - \text{H}$  charge exchange reaction.

For  $\text{H}_2$ , a marked non-equilibrium distribution of populations is established at  $z \approx 300$ , followed by a plateau involving levels from  $v = 1$  to 9. Levels above  $v = 9$  are excluded from this last plateau as their populations drop dramatically due to the endoergic character of the process of associative detachment (see Section 2.1). Therefore, when the thermal kinetic energy is much lower than the energy thresholds, the formation of highly excited ( $v \geq 10$ )  $\text{H}_2$  molecules is strongly suppressed. Such a strong splitting of level histories is not observed at higher  $z$ , since the main  $\text{H}_2$  formation mechanism ( $\text{H} + \text{H}_2^+$  charge transfer) is exoergic for all  $v$  (in contrast with the charge transfer  $\text{H}^+ + \text{H}_2$ , that is a threshold process).

The  $\text{H}_2$  vibrational distribution functions obtained at different values of the redshift are shown in Fig. 11, compared with the equilibrium curves corresponding to the Boltzmann vibrational distributions at the corresponding value of the gas temperatures. The shape of the level population distribution of  $\text{H}_2$  at low  $z$  can be understood and even roughly evaluated on the basis of a balance between radiative and formation rates. Indeed, the bunching of population of excited levels for low  $z$  is due to the fact that each population is determined essentially from the ratio of associative detachment and radiative rates.

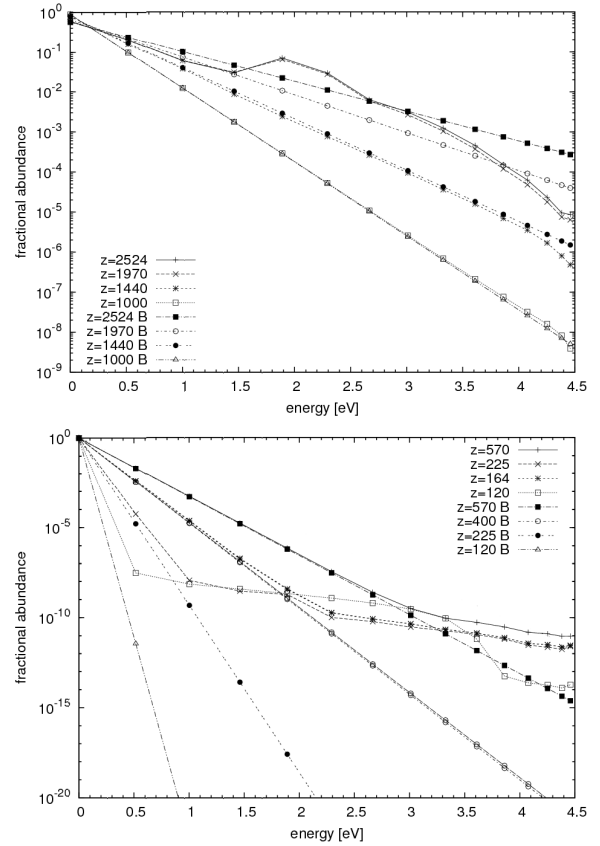


FIG. 11.— Vibrational level populations of  $\text{H}_2$ , normalized to the total  $\text{H}_2$  fractional abundance, at various redshifts. The Boltzmann distributions at each redshift are indicated with the label “B”.

The ratios for all exothermic channels ( $v < 10$ ) have comparable values on a enlarged logarithmic scale like that used here.

For  $\text{H}_2^+$ , the most relevant formation process is radiative association. The vibrational resolution of this species shows that the formation process, being faster for highly excited vibrational levels of the products, leads to a pronounced tail in the vibrational distribution (Fig. 12). The latter is characterized by a high population of the first few vibrational levels followed by a suprathermal tail, in qualitative agreement with the results of HP06 (see their Fig. 4). However, for HP06 the dominant formation process of  $\text{H}_2^+$  is via  $\text{HeH}^+$ . This result supports the claim of HP06 that the radiative association channel plays a minor role among formation pathways in their model. Also in this case, we observe a strong grouping of the fractional abundance of excited levels which is explained by the balance between state specific level production rates and radiative transitions to  $v = 0$ .

These findings suggest that the processes leading to redistribution of the vibrational quanta need further attention. This study is also appropriate here because such processes cannot be modeled in the framework of the usual, not state-resolved approach. In our case, such redistributing channels are V-T and spontaneous/stimulated radiative processes. In order to understand how these pathways effect the vibrational distribution of  $\text{H}_2$  and  $\text{H}_2^+$ , further numerical experiments have been performed in various regimes, corresponding to particular physical conditions. Fig. 13 shows the results obtained for the case in which radiative processes have



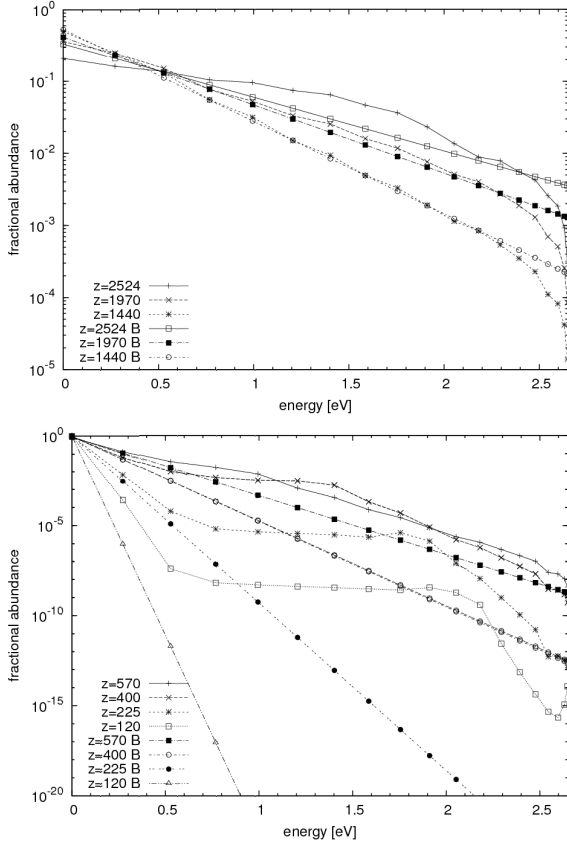


FIG. 12.— Same as Fig. 11 for  $\text{H}_2^+$ .

been omitted. The figure shows that, although radiative processes are not fast enough to thermalize level populations, they are essential to produce the actual vibrational distribution, and their neglect leads to complete different results especially at low  $z$ .

On the other hand, removal of V-T processes does not produce any appreciable variation with respect to the results of Fig. 10, since the rates of V-T processes are much smaller than the radiative ones. The role of V-T processes is better appreciated by looking at Fig. 14, where V-T processes and radiative decay are both ignored. Some variations with respect to Fig. 13 are observed: a higher vibrational temperature, a different high  $v$  plateau for  $\text{H}_2$ , especially at low  $z$ , and some differences of the total  $\text{H}_2^+$  fraction.

The main destruction channel (dissociative recombination) active at lower  $z$  is deeply affected by radiative processes: when these are ignored, the destruction channel becomes more efficient and the fractional abundance at the second peak (at  $z \sim 300$ ) is reduced by about a factor of 2. As a further check, removing radiative processes together with the loss channel leads to small variations of the fractional abundance. Thus, redistribution among levels is able to affect even the results for the total  $\text{H}_2^+$ , confirming the relevance of the non-equilibrium vibrational distributions.

No rotationally resolved data exists for most of the formation and destruction processes included in the present work, so a state-to-state kinetics cannot at the present stage go beyond the resolution of molecular vibrations. For  $\text{H}_2$  and  $\text{H}_2^+$ , the typical rotational energies are of the order of 0.01 eV: this suggests that the way in which ro-

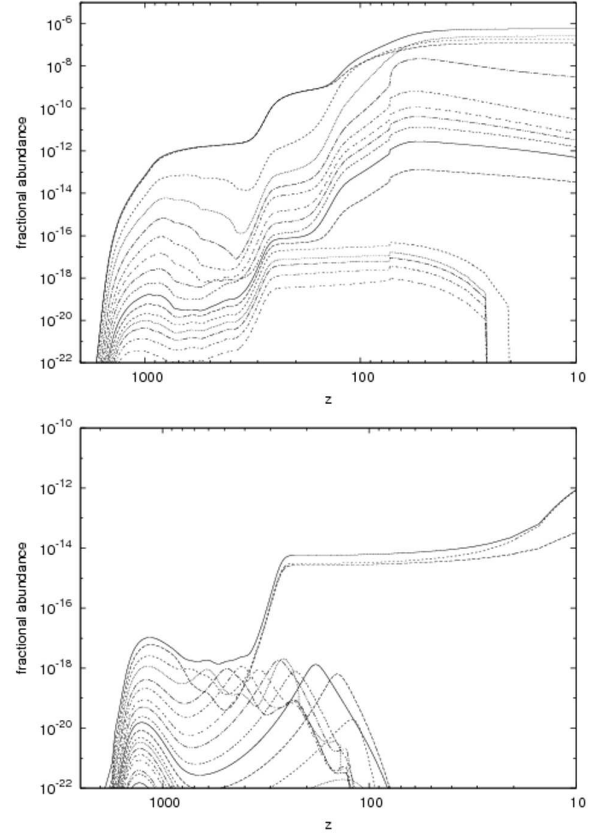


FIG. 13.— Same as Fig. 10, including formation and destruction channels, V-T processes but no radiative transition.

tation is included in the kinetic model can affect the low  $z$  trend of molecular abundance. To test the sensitivity of the chemical abundances to the rotational structure of  $\text{H}_2$  and  $\text{H}_2^+$ , we have computed the  $\text{H}_2^+$  radiative association rate coefficient (Subsection 2.3) assuming that the rotational manifold for each vibrational level reduces to only one  $J$ , either the lowest or the highest. Even if this hypothesis implies a very strong rotational non-equilibrium, it has negligible effect on the freeze-out value of  $\text{H}_2^+$ , although the abundance of this species at  $z \simeq 1000$  is changed. Furthermore, since the photodissociation cross section is not rotationally resolved, the rotational degree of freedom only enters in Eq.(2) through  $Z_{rot}$ . As a consequence, the nascent vibrational distribution function, which is the most important quantity here, is only marginally modified.

## 5. CONCLUSIONS

In this work we have performed calculations of the vibrational distribution of both  $\text{H}_2$  and  $\text{H}_2^+$  for the conditions expected in the early Universe and based on a comprehensive state-to-state chemical kinetics. The vibrational level distribution for these two species are reported for a wide and continuous range of the redshift parameter. The results can be summarized as follows:

1. The vibrational distribution function of  $\text{H}_2$  and  $\text{H}_2^+$  assumes a quasi-equilibrium shape at redshift  $z \sim 1500$ ; after that, extended plateau in the vibrational level distributions form, underlying the presence of pumping phenomena for the intermediate vibrational levels; full thermalization is not

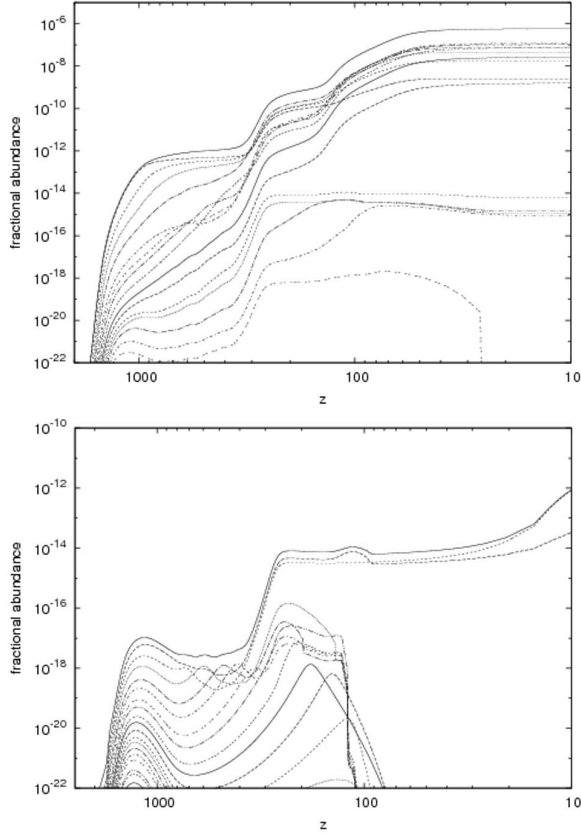


FIG. 14.— Same as Fig. 10, including formation and destruction channels, but no V-T process and radiative transition.

observed, because vibrational relaxation processes are not fast enough to balance the strong vibrational selectivity of formation rates.

2. Radiative processes play a fundamental role in the redistribution of vibrational quanta, affecting the vibrational distribution function and the overall fractional abundance (as in the case of  $\text{H}_2^+$ );
3. All these features can not be described in terms of the LTE distributions which are usually assumed in chemical networks for the primordial Universe.

We are grateful to the following colleagues for their precious aid in retrieving vibrationally resolved cross sections: Roberto Celiberto, Martin Čížek, Gordon Dunn, Fabrizio Esposito, Predrag Krstić, Ratko Janev, Ralph Jaquet, Susanta Mahapatra, Donald Shemansky, Hidekazu Takagi, Xavier Urbain. C.M.C. would also acknowledge Jonathan Tennyson and Ioan F. Schneider for useful discussions on electron–molecule collisions, and MIUR and Università degli Studi di Bari, that partially supported this work (“fondi di Ateneo 2010”).

## APPENDIX

### ANALYTICAL FITS OF LTE RATE COEFFICIENTS

In the present section, the analytic expressions of the vibrational LTE rate coefficients of the chemical processes introduced in the present model are reported. For processes that are vibrationally resolved in the final states, the sum on the entire final manifold has also been carried out.

TABLE 3  
CHEMICAL REACTIONS AND THEIR LTE RATE COEFFICIENTS

Chemical process	Rate coefficient (m <sup>3</sup> s <sup>-1</sup> ) or (s <sup>-1</sup> )
1] H + H <sup>-</sup> → H <sub>2</sub> (v) + e <sup>-</sup>	$\log_{10} k = \sum_{n=0}^2 a_{2n} [\log_{10}(T_{\text{gas}}/10^2)]^{2n}$ $a_0 = -14.4$ $a_2 = -0.15$ $a_4 = -7.9 \times 10^{-3}$
2] H <sub>2</sub> (v) + H <sup>+</sup> → H <sub>2</sub> <sup>+</sup> (v') + H	$\ln k = a_0 + a_1 T_{\text{gas}} + a_2/T_{\text{gas}} + a_3 T_{\text{gas}}^2$ , $a_0 = -33.081$ $a_1 = 6.3173 \times 10^{-5}$ $a_2 = -2.3478 \times 10^4$ $a_3 = -1.8691 \times 10^{-9}$
3] H <sub>2</sub> <sup>+</sup> (v) + H → H <sup>+</sup> + H + H	$\ln k = a_0 + a_1 T_{\text{gas}} + a_2/T_{\text{gas}} + a_3 T_{\text{gas}}^2$ , $a_0 = -32.912$ $a_1 = 6.9498 \times 10^{-5}$ $a_2 = -3.3248 \times 10^4$ $a_3 = -4.08 \times 10^{-9}$
4] H <sub>2</sub> (v) + H <sup>+</sup> → H + H + H <sup>+</sup>	$\ln k = a_0 + a_1 T_{\text{gas}} + a_2/T_{\text{gas}} + a_3 T_{\text{gas}}^2$ , $a_0 = -33.404$ $a_1 = 2.0148 \times 10^{-4}$ $a_2 = -5.2674 \times 10^4$ $a_3 = -1.0196 \times 10^{-8}$
5] H <sub>2</sub> (v) + H → H + H + H	$k = 1.9535 \times 10^{-10} T_{\text{gas}}^{-0.93267} \exp(-4.9743 \times 10^4/T_{\text{gas}})$
6] H <sub>2</sub> (v) + hν → H <sub>2</sub> <sup>+</sup> (v') + e <sup>-</sup>	$k = 3.06587 \times 10^9 \exp(-1.89481 \times 10^5/T_{\text{gas}})$
7] H <sub>2</sub> (v) + hν → H + H (indirect)	$\ln k = 17.555 + 7.2643 \times 10^{-6} T_{\text{gas}} - 1.4194 \times 10^5/T_{\text{gas}}$
8] H <sub>2</sub> <sup>+</sup> (v) + e <sup>-</sup> → 2H	$k = \sum_{n=0}^5 a_n T_{\text{gas}}^n$ , $a_0 = 4.2278 \times 10^{-14}$ $a_1 = -2.3088 \times 10^{-17}$ $a_2 = 7.3428 \times 10^{-21}$ $a_3 = -7.5474 \times 10^{-25}$ $a_4 = 3.3468 \times 10^{-29}$ $a_5 = -5.528 \times 10^{-34}$
9] H <sup>-</sup> + hν → H + e <sup>-</sup>	$k = 0.11 T_{\text{rad}}^{2.13} \exp(-8.823 \times 10^3/T_{\text{rad}})$ $k = 8.0 \times 10^{-8} T_{\text{rad}}^{1.3} \exp(-2.3 \times 10^3/T_{\text{rad}})$ (non-thermal)

## REFERENCES

- Allison, A. C., Dalgarno, A., 1969, *Atom. Data & Nucl. Data Tables*, 1, 91
- Allison, A. C., Dalgarno, A., 1970, *Atom. Data & Nucl. Data Tables*, 1, 289
- Anninos, P., Norman, M. L. 1996, *ApJ*, 460, 556
- Argyros J.D., 1974, *J. Phys. B* 7, 2025
- Balakrishnan, N., Vieira, M., Babb, J. F., Dalgarno, A., Forrey R. C., Lepp S., 1999, *ApJ*, 524, 1122
- Bieniek, R. J., Dalgarno, A., 1979, *ApJ*, 228, 635
- Capitelli, M., Coppola, C. M., Diomede, P., Longo, S., 2007, *A&A*, 470, 811
- Celiberto, R., Janev, R. K., Laricchiuta, A., Capitelli, M., Wadhera, J. M., Atems D.E., 2001, *Atom. Data & Nucl. Data Tables*, 77,161
- Cherchneff, I., Lilly, S., 2008, *ApJ*, 683, L123
- Čížek, M., Horáček, J., Domcke, W., 1998, *J. Phys. B: Atom., Molec. & Opt. Phys.*, 31, 2571
- Clark, A. P., 1977, *J. Phys. B: Atom., Molec. & Opt. Phys.*, 10, L389
- Coppola, C. M., Diomede, P., Longo, S., Capitelli, M. 2011, *ApJ*, 727, 37
- Dalgarno, A., Stephens, T. L., 1970, *ApJ*, 160, L107
- Dalgarno, A., 2005, *J. of Phys., Conf. Ser.*, 4, 10
- Dunn, G., 1968, *Phys. Rev.*, 172, 1
- Esposito, F., Gorse, C., Capitelli, M., 1999, *Chem. Phys. Lett.*, 303, 636
- Esposito, F., Capitelli, M., 2001, *Atomic and Plasma-Material Interaction Data for Fusion*, 9, 65
- Fano, U., 1961, *Phys. Rev.*, 124, 1866
- Fantz, U., Wunderlich, D., 2006, *Atom. Data & Nucl. Data Tables*, 92, 853
- Fifrig, M., Stroe, M., 2008, *Phys. Scripta*, 78, 065302(1)
- Flannery, M. R., Tai, H., Albritton, D. L., 1977, *Atom. Data & Nucl. Data Tables*, 20, 563
- Flower, D., Roueff, E., Zeippen, C. J., 1998, *J. of Phys. B: Atom., Molec. & Opt. Phys.*, 31, 1105
- Flower, D., 2000, *A&A*, 362, 774
- Galli, D., Palla, F., 1998, *A&A*, 335, 403 (GP98)
- Glass-Maujean, M., 1986, *Phys. Rev. A*, 33, 1, 342
- Glover, S. C. O., Jappsen, A. K., 2007, *ApJ*, 666, 1
- Glover, S. C. O., Abel, T. 2008, *MNRAS*, 388, 1627
- Hirata, C. M., Padmanabhan, N., 2006, *MNRAS*, 372, 1175 (HP06)
- Hunter, G., Yau, A. W., Pritchard, H. O., 1974, *Atom. Data & Nucl. Data Tables*, 14, 11
- Karpas Z., Anicich V., Huntress W. T., 1979, *J. of Chem. Phys.*, 70, 2877
- Khersonski, V. K., 1982, *Astrophys. & Sp. Sci.*, 88, 21
- Kolos, W., Wolniewicz, L., 1964, *J. Chem. Phys.*, 41, 3674
- Komatsu, E., Dunkley, J., Nolte, M. R., Bennett, L., Gold, C. B., G. Hinshaw, Jarosik, N., Larson, D., Limon, M., Page, L., Spergel, D. N., Halpern, M., Hill, R. S., Kogut, A., Meyer, S. S., Tucker, G. S., Weiland, J. L., Wollack, E., Wright, E. L., 2009, *ApJS*, 180, 2, 330
- Krstić, P. S., Schultz, D. R., 1999, *J. Phys. B: Atom., Molec. & Opt. Phys.*, 32, 2415
- Krstić, P. S., Schultz, D. R., Janev, R. K., 2002, *Phys. Scripta*, T96, 61
- Krstić, P. S., 2002, *Phys. Rev. A*, 66, 042717(1)
- Krstić, P. S., 2003, *Phys. Rev. A*, 67, 022708(1)
- Krstić, P. S., 2005, *Nucl. Instr. & Meth. in Phys. Res. B*, 241, 58
- Lebedev, V. S., Presnyakov, L. P., Sobel'man, I. I., 2000, *Astr. Rep.*, 11, 5, 338
- Lebedev, V. S., Presnyakov, L. P., Sobel'man, I. I., 2003, *Physics-Uspekhi*, 46, 5, 473
- Launay, J. M., Le Dourneuf, M., Zeippen, C.J., 1991, *A&A*, 252, 842
- Lee, T. G., Rochow, C., Martin, R., Clark, T. K., Forrey, R. C., Balakrishnan, N., Stancil, P. C., Schultz, D. R., Dalgarno, A., Ferland, G. J., 2005, *J. Chem. Phys.*, 122, 024307/1
- Lepp, S., Stancil, P. C., Dalgarno, A., 2002, *J. Phys. B: Atom., Molec. & Opt. Phys.*, 35, R57
- Lewis Ford, A., Docken, K. K., Dalgarno, A., 1975, *ApJ*, 195, 819
- Linder, F., Janev, R. K., Botero, J. 1995, *Atomic & Molecular Processes in Fusion Edge Plasmas*, 397
- Liu, X., Shemansky, D. E., 2004, *ApJ*, 614, 1132
- Motapon, O., Tamo, F. O. W., Urbain, X., Schneider, I. F. 2008, *Phys. Rev. A*, 77, 5
- ONeil, S. V., Reinhardt, W. P., 1978, *J. Chem. Phys.*, 69, 5, 2126
- Pagel, B. E., 1959, *MNRAS*, 119, 609
- Posen, A. G., Dalgarno, A., Peek, J. M., 1983, *Atom. Data & Nucl. Data Tables*, 28, 2, 265
- Puy, D., Signore, M. 2007, *NewAR*, 51, 411
- Ramaker, D. E., Peek, J. M., 1976, *Phys. Rev. A*, 13, 1, 58
- Savin, D. W., Krstić, P. S., Haiman, Z., Stancil, P. C. 2004, *ApJ*, 606, L167
- Schleicher, D. R., Galli, D., Palla, F., Camenzind, M., Klessen, R. S., Bartelmann, M., Glover, S. C. O., 2008, *A&A*, 490, 521 (S08)
- Schneider, I. F., Dulieu, O., Giusti-Suzor, A., Roueff, E., 1994, *ApJ*, 424, 983 (errata in *ApJ* 486, 580)
- Seager, S., Sasselov, D. D., & Scott, D. 1999, *ApJ*, 523, L1
- Seager, S., Sasselov, D. D., Scott, D., 2000, *ApJS*, 128, 407
- Shapiro, P. R., Kang, H., 1987, *ApJ*, 318, 32
- Stancil, P. C., Babb, J. F., Dalgarno, A., 1993, *ApJ*, 414, 672
- Stancil P.C., 1994, *ApJ* 430, 360
- Stancil, P. C., Lepp, S., Dalgarno, A., 1998, *ApJ*, 509, 1
- Stroe, M., Fifrig, M., 2009, *J. Phys. B: Atom., Molec. & Opt. Phys.*, 42, 205203
- Tai, H., Flannery, M. R., 1977, *Phys. Rev. A*, 16, 3, 1124
- Takagi, H., Hara, S., Sato, H., 2009, *Phys. Rev. A*, 79, 012715(1)
- Takagi, H., 2002, *Phys. Scripta*, T96, 52
- Turner, J., Docken, K. K., Dalgarno, A., 1977, *ApJS*, 35, 281
- Vonlanthen, P., Rauscher, T., Winteler, C., Puy, D., Signore, M., Dubrovich, V., 2009, *A&A*, 503, 47
- Wolniewicz, L., Simbotin, I., Dalgarno, A., 1998, *ApJS*, 115, 293
- Wong, W. Y., Moss, A., Scott, D., 2008, *MNRAS*, 386, 1023
- Yousif, F. B., Mitchell, J. B. A., 1995, *Zeitschrift für Physik D: Atoms, Molecules and Clusters*, 34, 195
- Zucker, C. W., Eyler, E. E., 1986, *J. Chem. Phys.*, 85, 12, 7180